arXiv:1704.05111v1 [physics.atom-ph] 17 Apr 2017

Infrared and visible laser spectroscopy for highly-charged Ni-like ions

Yuri Ralchenko

Quantum Measurement Division, National Institute of Standards and Technology, Gaithersburg, MD 20899-8422, USA

Abstract

Application of visible or infrared (IR) lasers for spectroscopy of highly-charged ions (HCI) has not been particularly extensive so far due to a mismatch in typical energies. We show here that the energy difference between the two lowest levels within the first excited configuration $3d^9 4s$ in Ni-like ions of heavy elements from Z_N=60 to Z_N=92 is within the range of visible or near-IR lasers. The wavelengths of these transitions are calculated within the relativistic model potential formalism and compared with other theoretical and limited experimental data. Detailed collisional-radiative simulations of non-Maxwellian and thermal plasmas are performed showing that photopumping between these levels using relatively moderate lasers is sufficient to provide a two-order of magnitude increase of the pumped level population. This accordingly results in a similar rise of the x-ray line intensity thereby allowing control of x-ray emission with visible/IR lasers.

Keywords: `Ni-like ions, visible and infrared lasers, spectroscopy`

Laser spectroscopy [1] has become one of the most exciting and successful fields of research. Its ubiquitous applications extend from laser-induced breakdown spectroscopy (LIBS) to laser cooling of atoms and molecules to optical lattices, to name a few. In practically all applications it is the neutral or low-charge atoms (or molecules) that are the subject of visible or infrared (IR) laser

Email address: `yuri.ralchenko@nist.gov` (Yuri Ralchenko)

research. Since characteristic energy differences for ions rapidly grow with ion charge z, typically as z (Coulomb interactions) or even z^4 (spin-orbit interaction) for Δn=0 transitions (here n is the principal quantum number) and z^2 for $\Delta n \neq 0$, common lasers with photon energies on the order of 0.5 eV to 3 eV cannot be easily used for spectroscopy of mid- and high-charge ions. While the recently developed x-ray free-electron lasers (XFEL) [2] open a new chapter in laser spectroscopy with highly-charged ions, the significant cost of XFELs prohibits their widespread utilization in research.

Some highly-charged atomic ions may exhibit fine or hyperfine structure of the ground configuration with energy differences within reach of traditional lasers. One example is the B-like ion Ar^{13+} with the ground configuration $2s^2 2p$. Although the J=1/2 and J=3/2 levels of this configuration are connected by a forbidden magnetic-dipole (M1) rather than an allowed electric-dipole (E1) transition, a modest combination of a pulsed 100-Hz Nd:YAG laser pumping a dye laser with a power of up to 1.2 W was sufficient to photoexcite the 2.8-eV $2p_{3/2}$-$2p_{1/2}$ transition and accurately measure its wavelength [3]. With the ion charge increase, as mentioned above, this energy difference grows fast so that for B-like Fe^{21+} it is about 14.7 eV, while for B-like Ba it reaches about 420 eV. Another example of application of visible laser spectroscopy in highly-charged ions research is the recent measurement of the hyperfine ground-configuration transitions in H-like and Li-like ions of Bi [4].

In addition to the wavelength constraints, an effective interaction between laser photons and an atom or an ion can only be reached when the lower photoexcited state has a substantial population. Due to an infinite number of converging atomic states (here we ignore continuum lowering effects in dense plasmas), one can find transitions with almost any energy that is smaller than the corresponding ionization potential. However, the populations of low excited states are generally rather small due to possible E1 radiative decays with fast rates that scale as z^4. The higher excited states in plasmas experience strong collisions and therefore photoexcitation would be too weak to affect their populations. The low metastable states certainly have larger populations than other

excited states, however, since forbidden radiative probabilities increase with z even faster than the E1 rates, in highly-charged ions they may also be too depleted radiatively to be used in laser photoexcitation studies. Fortunately, as will be discussed below, some lowest metastable states in highly-charged ions have very small radiative decay rates and thus their populations are extremely high.

In this paper we analyze applicability of visible and near-IR lasers to spectroscopy of highly-charged ions in the Ni-like isoelectronic sequence. Although the ground configuration of neutral Ni is $3d^8 4s^2$, it becomes a closed-shell configuration $3d^{10}$ for all other members of the isoelectronic sequence [5]. The first excited configuration above the single $J = 0$ level of $3d^{10}$ is $3d^9 4s$ with the four levels having the following values of the total angular momentum (in the increasing order of energies): 3, 2, 1, and 2 (see Fig. 1 for the level structure of the $3d^9 4s$ configuration in Ni-like W^{46+}). For highly-charged ions, this configuration clearly exhibits jj-coupling, which results in doublet grouping of the 3-2 and 1-2 pairs of levels. For instance, in Ni-like tungsten the energy difference between the two doublets is about 40 times larger than their corresponding splittings [5].

Since $3d^9 4s$ has the same parity as $3d^{10}$, there exist no allowed E1 transitions between these configurations. However, the forbidden $3l - 4l'$ transitions of different multipoles become strong enough to overcome collisional destruction in low-density plasmas and result in detectable spectral lines even in laser-produced plasmas (see, e.g., [6]). Although electric-quadrupole (E2) transitions have the highest decay rate, even the magnetic-octupole (M3) line $3d^{10}$–$3d^9 4s$ $(5/2,1/2)_3$ was reliably observed under low densities ($n_e \approx 10^{11}$ cm^{-3}) of electron beam ion traps (EBIT) already 25 years ago [7]. Also, the M1 transitions from the J=1 $3d^9 4s$ levels have too small branching ratios to be of any importance for the following discussion.

Over the last decade the $3d^{10}$–$3d^9 4s$ E2 and M3 lines in Ni-like W^{46+} have been a subject of extensive analysis, in part due to importance of tungsten for ITER research (e.g., [8]). The low-resolution tokamak and EBIT measurements

[9, 10] recorded an unresolved spectral feature due to an overlap of these two close lines near 0.74 nm. The first attempt at modeling W^{46+} emission with the ADAS package [9] was not particularly successful in explaining the observed intensity although a more detailed large-scale modeling of EBIT spectra [10] resulted in a much better agreement with the measurements. It was explained later in Ref. [11] that the J=3 and J=2 levels of $3d^9 4s$ that are connected by a very weak M1 transition become strongly coupled via collisional-radiative interaction with the intermediate configuration $3d^9 4p$. Consequently, the population of the lower metastable J=3 level may be transferred to the J=2 level via excitation followed by a radiative decay. Furthermore, the ratio of M3 and E2 line intensities in Ni-like W was shown to be strongly dependent on electron density in the range of values relevant to magnetic fusion devices [11]. The experimental work on these lines culminated with high-resolution measurements at LLNL EBIT [12] that yielded observed wavelengths of 0.79374 nm for M3 and 0.79280 nm for E2 with a better than 0.01% accuracy. That work also showed that the measured intensities of the M3 and E2 lines are comparable in magnitude. Since radiative probabilities for these high-multipole transitions differ by many orders (e.g., about 10^6 for Ni-like tungsten [11]), it follows then that the population of the J=3 level is larger than that of the J=2 level by about the same factor. Therefore, one may expect that photoexcitation of a very small fraction of population of the J=3 level should result in a significant increase of the J=2 population and, accordingly, the intensity of the E2 line.

While the energy differences for the J=3 and J=2 levels derived from the already measured spectral lines in Ni-like W, Th, and U are in the visible range, it is helpful to analyze their dependence along the isoelectronic sequence. Figure 2 presents calculated and measured wavelengths for the J=3–J=2 M1 transition in Ni-like ions for the range of nuclear charges $Z_N = 60$ to 93. Our calculations were performed using the Flexible Atomic Code (FAC) [13] (squares). FAC implements the relativistic model potential method to calculate wavefunctions and other atomic characteristics such as energies, radiative transition probabilities, and electron-impact cross sections. Important quantum-electrodynamic effects,

e.g., Breit interaction, are added as well. The relativistic many-body perturbation theory (RMBPT) calculations of Ref. [14] are presented by diamonds. The experimental data for W, Th, and U are derived from the M3 and E2 wavelength measurements performed at the LLNL EBIT [7, 12]. The uncertainties for the W data point are so small that the error bars are within the symbol.

The measured and calculated wavelengths are seen to agree very well. Obviously, the large uncertainties for the old Th and U data points make it more difficult to quantify the disagreement but for W, the experimental and FAC wavelengths agree within 3%. This is a relatively large discrepancy for typical atomic structure calculations but here the wavelengths are determined from the differences of two large excitation energies, and thus the ensuing uncertainties become larger. Nonetheless, it is clear that the wavelengths for this transition are in the near-infrared and visible parts of spectra across the entire range of nuclear charges from 60 to 93. The z dependence of the wavelength is rather weak, about $1/z$, which is typical for $\Delta n = 0$ transitions. The value of the M1 oscillator strength shown in figure 2 (right y-axis) is rather small, on the order of 2×10^{-7}, which is not unexpected for forbidden transitions with energy differences of a few eV. For comparison, the f-value for the 441-nm Ar^{13+} M1 photoexcitation transition [3] was only about factor of 5 larger. Note also that the radiative probabilities for the J=3–J=2 M1 transitions vary between 20 s^{-1} and 120 s^{-1}, and thus they are completely negligible in population kinetics for these levels.

While the wavelength of the M1 transition between the levels can be easily matched by various lasers, the photoexcitation from J=3 to J=2 cannot be effective above a specific value of electron density that varies along the isoelectronic sequence. In Ref. [11] (see also [7]) it was shown in much detail that at higher densities a collisional-radiative (CR) redistribution of population from J=3 into J=2 via $3d^9 4p$ levels efficiently depletes the lower level. In figure 3 we present the calculated ratio of the M3 and E2 line intensities for a number of Ni-like ions from Z_N=50 Sn to Z_N=92 U in steady-state Maxwellian plasmas with temperatures of about the ionization potential of the corresponding Ni-

like ion. As discussed in [15], for highly-charged high-Z elements the electron temperatures required to reach maximal abundance for a specific ion are on the order or even larger than its ionization potential. The CR simulations were performed with the code NOMAD [16, 17] using atomic data (energy levels, radiative transition probabilities, electron-impact cross sections for excitation, ionization, and recombination) calculated with FAC. The model includes Cu-, Ni-, and Co-like ions which allows us to account for practically all important physical processes affecting populations of the lowest excited levels in Ni-like ions. The CR calculations show that at some value of the electron density (from 10^8 cm^{-3} for Sn to 10^{14} cm^{-3} for U) the electron-impact excitation rate $3d^9 4s$–$3d^9 4p$ becomes comparable with the weak M3 transition probability and thus the J=3 level does not live long enough to reach the corresponding radiative lifetime. In figure 3 this change in primary depopulation process for J=3 corresponds to a sharp decrease of the intensity ratio. Therefore, above these density limits the populations of the lower level are generally too small to be used for photoexcitation.

In order to calculate the effect of laser photoexcitation on populations of the J=3 and J=2 levels, one has to perform a full time-dependent CR modeling. Here again the NOMAD code [16] is applied to simulation for tungsten ions in tokamaks and EBITs. The plasma parameters for EBIT conditions are n_e=10^{11} cm^{-3} with an electron beam energy distribution represented by a Gaussian function centered at 3950 eV and full width at half maximum (FWHM) of 40 eV. For a Maxwellian tokamak plasma the corresponding parameters were n_e=10^{13} cm^{-3} and electron temperature T_e=4200 eV. These values of temperatures and beam energies provide significant abundance for Ni-like ions of tungsten. Collisions with protons in tokamak plasmas may provide some contribution to equilibration between the levels of interest that dissappears in the low density limit; while this effect should in principle be clarified, here we neglect it emphasizing the electron collisions. In both cases the simulation starts from a steady-state condition at time t=0 and continues until t=10^{-2} s using a logarithmic grid of 150 steps. A laser with a wavelength of 629.186 nm corresponding

to the calculated energy difference, FWHM of 0.024 nm, and intensity of 10^7 W/cm^2 was ssumed to illuminate the plasma from t=10^{-12} s either continuously until the final time or in a pulse mode until 10^{-8} s.

The simulation results for the relative (normalized to the steady-state value at t=0) population of the J=2 level are presented in figure 4. As soon as the laser is turned on, the photoexcitation J=3→J=2 provides a very strong population flux that increases the upper level population by more than two orders of magnitude for both plasmas within just 1 ns. As mentioned above, such a significant contribution is due to a very large imbalance of populations between two levels. This equilibration time is on the order of the radiative lifetime of the J=2 transition into the ground state which is the fastest physical process among all possible depopulation mechanisms for this level. The same lifetime gives an estimate of the relaxation time in the pulse-mode simulation when the laser is turned off at 10 ns (inset in figure 4). The drop in population above 100 ns, in turn, is related to depletion of the J=3 level due to photoexcitation with a rate of 4×10^6 s^{-1}. At asymptotically large times, the relative population limit reflects the established equilibration between the two levels when the radiative decay of J=3 with the probability of about 1000 s^{-1} is completely negligible compared to laser photoexcitation.

To summarize, the presented calculations show that the energy difference between the lowest excited levels within the $3d^9 4s$ configurations in Ni-like high-Z ions is within a few eV, which allows one to use it for photopumping with visible or near-infrared lasers. Moreover, our time-dependent collisional-radiative simulations for Ni-like W show that such photoexcitation increases the population of the J=2 level by more than two orders of magnitude and thus may result in observable detection of enhanced x-ray emission in the E2 transition into the ground state. Such a mechanism may allow control of x-ray emission in hot plasmas of Ni-like ions with the standard laser techniques from laser spectroscopy. Without loss of generality, we can assume that similar effects can be observed in other Ni-like ions of heavy elements.

The author is grateful to U.I. Safronova for providing detailed energy levels

for Ni-like ions from Ref. [14] and to E. Stambulchik and A. Kramida for valuable comments. The FAC input files used to calculate the atomic data are available on request.

References

References

[1] W. Demtröder, Laser Spectroscopy, vols. 1 and 2 (Springer-Verlag Berlin Heidelberg, 2014, 2015).

[2] B. W. J. McNeil and N. R. Thompson, Nature Photonics 4, 814 (2010).

[3] V. Mäckel et al, Phys. Rev. Lett. 107, 143012 (2011).

[4] M. Lochmann et al, Phys. Rev. A 90, 030501 (2014).

[5] A. Kramida, Yu. Ralchenko, J. Reader and NIST ASD Team, NIST Atomic Spectra Database (ver. 5.4), [Online]. Available: `http://physics.nist.gov/asd` [2016, November 28]. National Institute of Standards and Technology, Gaithersburg, MD, 2016.

[6] J.-F. Wyart et al, Phys. Rev. A 34, 701 (1986).

[7] P. Beiersdorfer, A.L. Osterheld, J. Scofield, B. Wargelin, and R.E. Marrs, Phys. Rev. Lett. 67, 2272 (1991).

[8] R. Neu, ASDEX Upgrade Team, EU PWI Taskforce, and JET EFDA Contributors, Plasma Phys. Contr. Fus. 53, n.12 (2011).

[9] T. Pütterich, R. Neu, C. Beidermann, R. Radtke and ASDEX Upgrade Team, J. Phys. B 38, 3071 (2005).

[10] Yu. Ralchenko, J.N. Tan, J.D. Gillaspy, J.M. Pomeroy and E. Silver, Phys. Rev. A 74, 042514 (2006).

[11] Yu. Ralchenko, J. Phys. B 40, F175 (2007).

[12] J. Clementson, P. Beiersdorfer, and M.F. Gu, Phys. Rev. A 81, 012505 (2010).

[13] M.F. Gu, Can. J. Phys. 86, 675 (2008).

[14] U.I. Safronova, A.S. Safronova, S.M. Hamasha and P. Beiersdorfer, At. Data Nucl. Data Tables 92, 47 (2006).

[15] Yu. Ralchenko et al, in Atomic Processes in Plasmas, ed. by K. B. Fournier (AIP Conference Proceedings 1161, 2009), p. 242.

[16] Yu.V. Ralchenko and Y. Maron, J. Quant. Spectr. Rad. Transf. 71, 609 (2001).

[17] Modern Methods in Collisional-Radiative Modeling of Plasmas, ed. by Yu. Ralchenko (Springer International Publishing Switzerland, 2016).

List of figure captions:

Figure 1. (Colour online.) Levels of the $3d^9 4s$ configuration in Ni-like W^{46+} [5]. The doublet structure typical for jj-coupling is clearly visible. The transition energy of 1.87 eV between the J=3 and J=2 levels corresponds to the photon wavelength of 663 nm.

Figure 2. (Colour online.) The calculated (present work as squares and [14] as diamonds) and measured (solid circles) [7, 12] wavelengths for the J=3–J=2 transitions in Ni-like ions. The corresponding magnetic-dipole oscillator strengths (solid line, right y-axis) are shown in units of 10^{-7}.

Figure 3. (Colour online.) The intensity ratios between M3 and E2 transitions in Ni-like ions of Sn, Nd, Ho, W, and U as functions of electron density.

Figure 4. (Colour online.) Relative populations of the J=2 level (with regard to the steady-state population) under continuous laser photopumping starting at t=10^{-12} s. Solid line: Maxwellian plasma at 4200 eV and electron density $n_e = 10^{13}$ cm^{-3}; dashed line: Gaussian electron energy distribution at 3950 eV and $n_e = 10^{11}$ cm^{-3}. Inset: same plasma conditions but the laser is turned off at 10^{-8} s.

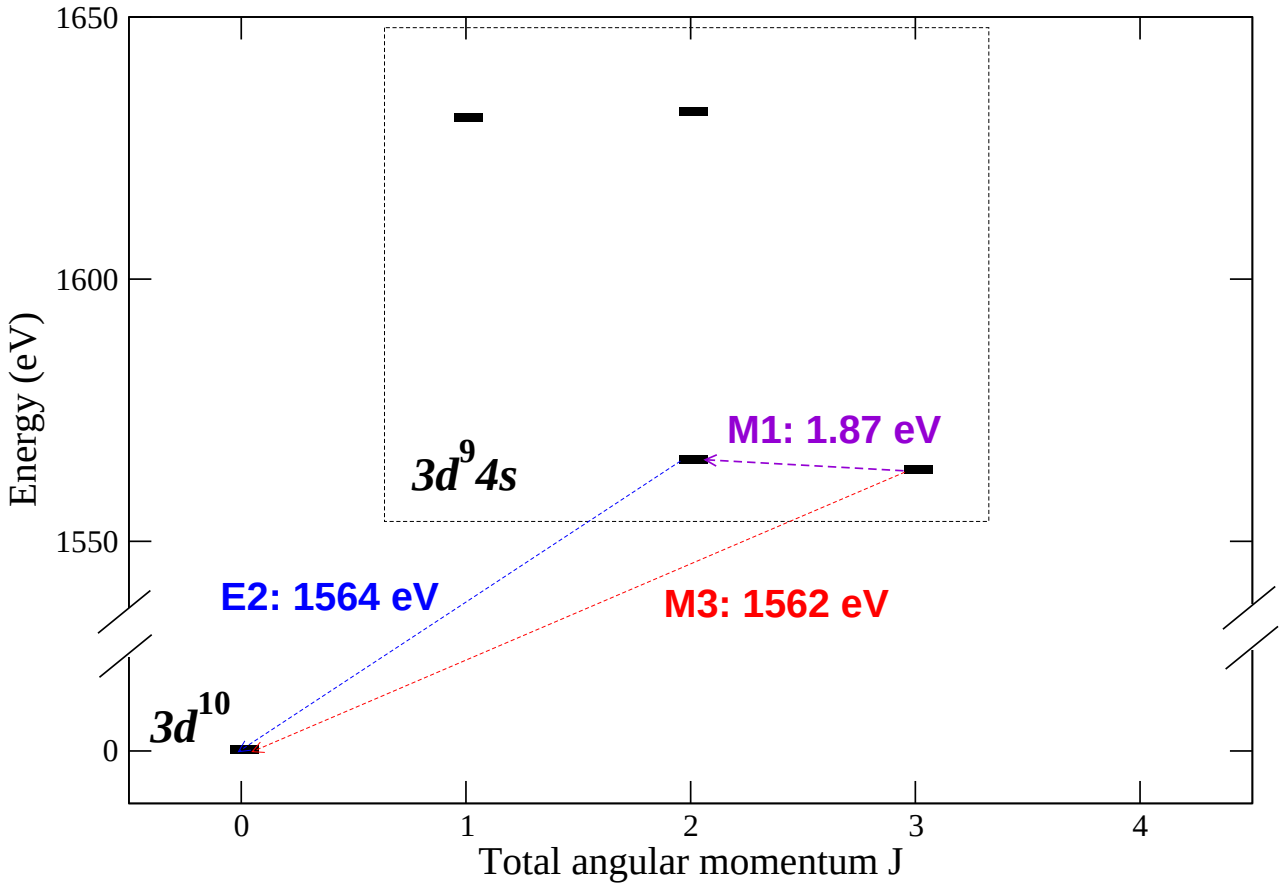
1650
1600
1550
0
Energy (eV)
$3d^9 4s$
M1: 1.87 eV
E2: 1564 eV
M3: 1562 eV
$3d^{10}$
0
1
2
3
4
Total angular momentum J

Figure 1:

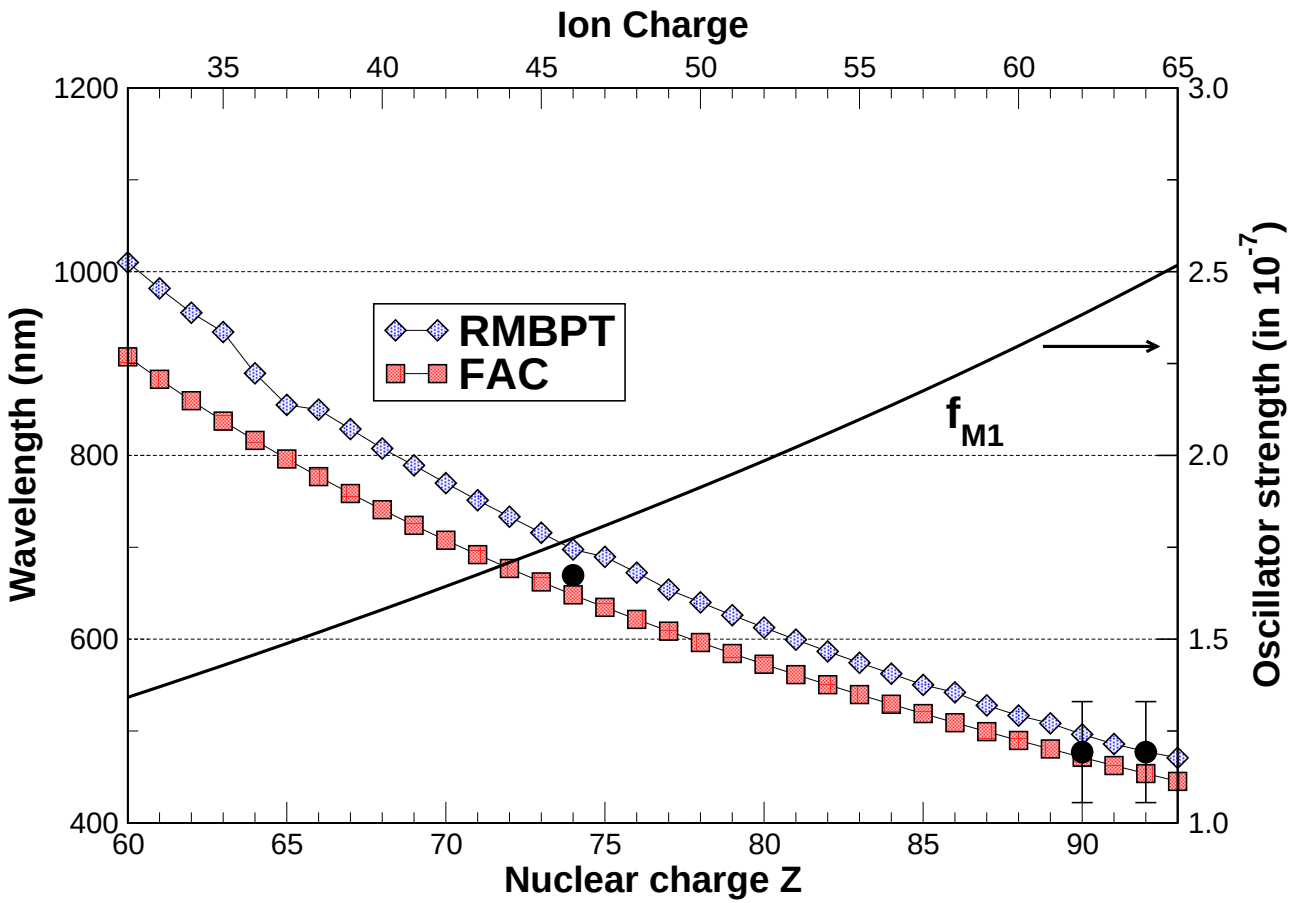
Ion Charge
35
40
45
50
55
60
65
1200
1000
800
600
400
3.0
2.5
2.0
1.5
1.0
Wavelength (nm)
Oscillator strength (in 10^-7)
RMBPT
FAC
f_M1
60
65
70
75
80
85
90
Nuclear charge Z

Figure 2:

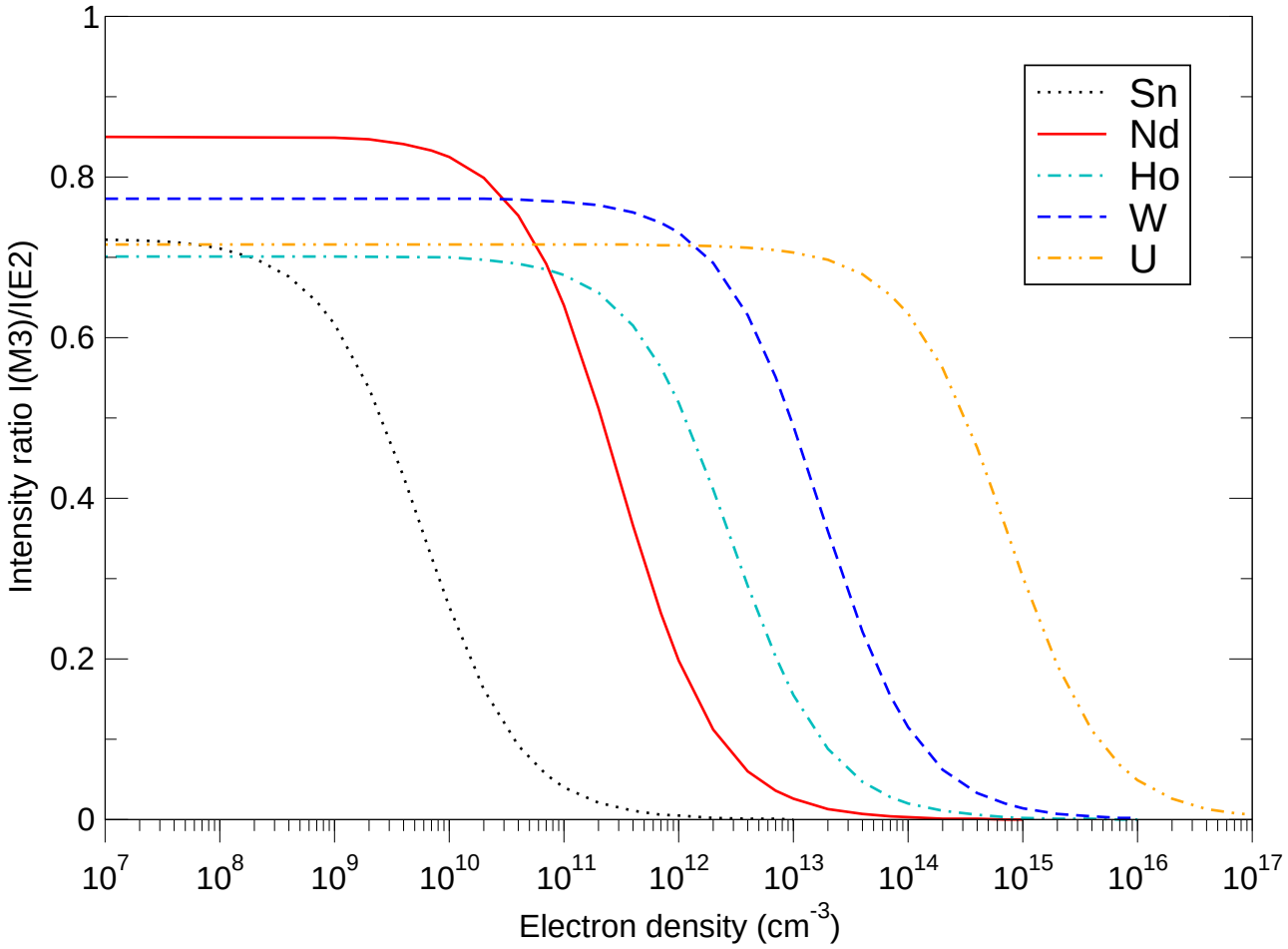
Intensity ratio I(M3)/I(E2)
Electron density (cm-3)
Sn
Nd
Ho
W
U
0
0.2
0.4
0.6
0.8
1
10^7
10^8
10^9
10^10
10^11
10^12
10^13
10^14
10^15
10^16
10^17

Figure 3:

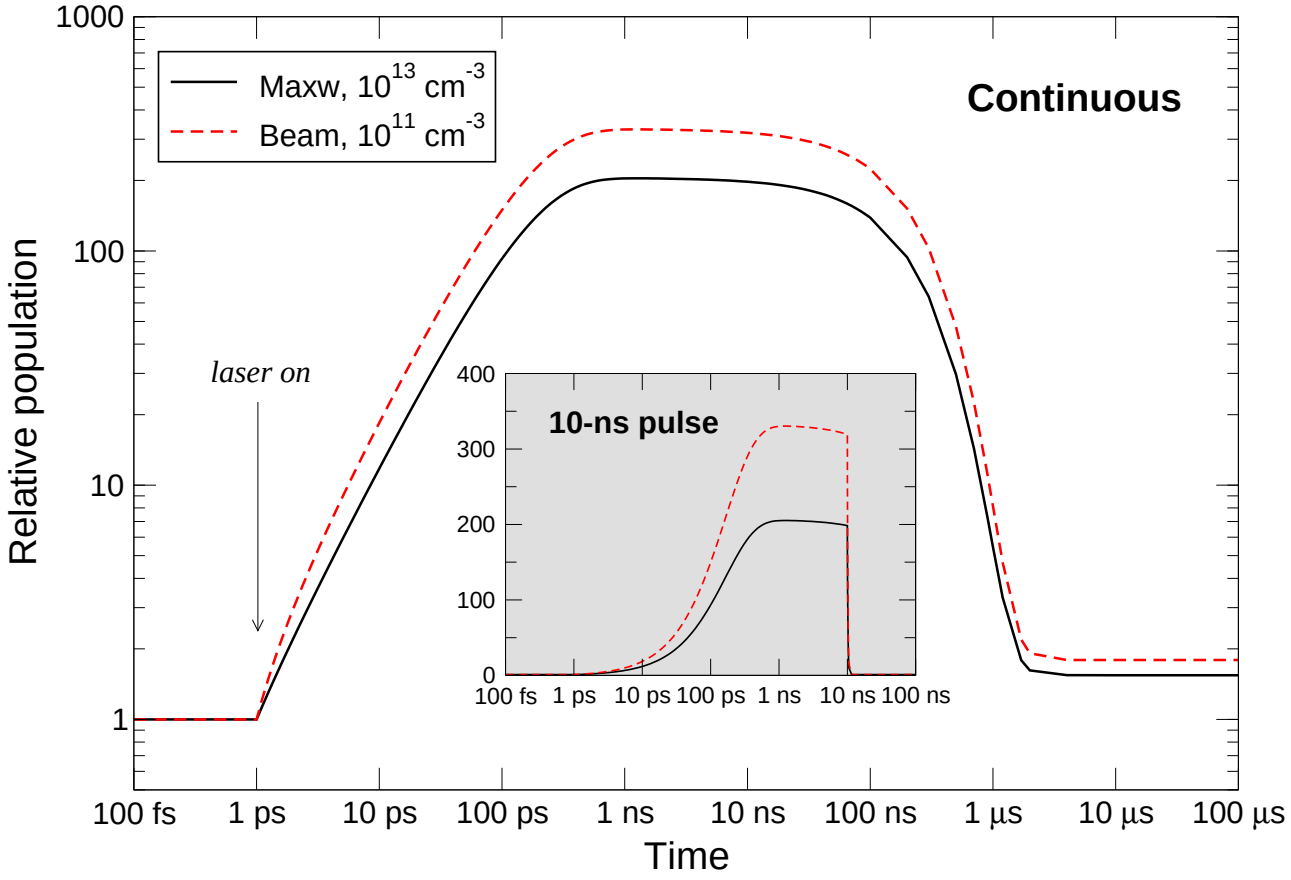
Maxw, 10^13 cm^-3
Beam, 10^11 cm^-3
Continuous
laser on
10-ns pulse
Relative population
Time
1000
100
10
1
400
300
200
100
0
100 fs
1 ps
10 ps
100 ps
1 ns
10 ns
100 ns
1 µs
10 µs
100 µs

Figure 4: